Article

Early Age Carbonation of Fiber-Cement Composites under Real Processing Conditions: A Parametric Investigation

Bundit Kottititum [1,2]**, Quoc Tri Phung** [2,*] (ID)**, Norbert Maes** [2]**, Wichit Prakaypan** [3] **and Thongchai Srinophakun** [1,*]

[1]   Department of Chemical Engineering, Kasetsart University, Bangkok 10900, Thailand; bundit.kottititum@sckcen.be
[2]   Institute for Environment, Health, and Safety, Belgian Nuclear Research Centre (SCK•CEN), 2400 Mol, Belgium; norbert.maes@sckcen.be
[3]   Mahaphant Fibre-Cement Public Company Limited, Lopburi 15220, Thailand; wichit_p@sherasolution.com
*   Correspondence: quoc.tri.phung@sckcen.be (Q.T.P.); fengtcs@ku.ac.th (T.S.); Tel.: +32-1433-3240 (Q.T.P.); +66-(2)-797-0999 (T.S.)

Abstract: This paper presents the outcome of a comprehensive experimental program undertaken to study the performance of cellulose pulp and synthetic PVA (polyvinyl alcohol) based fiber-cement composite under both carbonated and non-carbonated curing conditions at early age. The composites were produced at different rolling pressures (2.5 to 9.0 bar) and subjected to various curing conditions in which the effects of CO_2 pressure (1 to 3 bar) and curing time (3 to 9 h) were studied. The mechanical properties (modulus of elasticity (MOE), modulus of rupture (MOR), and toughness), as well as the physical properties (porosity, bulk density, and water absorption), were measured for all samples. Scanning electron microscopy (SEM) was used to investigate the effect of carbonation on porosity change and adhesion of fiber-matrix. A parametric investigation of the effects of the carbonation curing period, CO_2 pressure, and rolling pressure on the improvement of the physical and mechanical properties during carbonation curing was performed. Results showed that fiber-cement composites cured with an elevated CO_2 pressure of 3 bar, rolling pressure of 3 bar, and 5 h of curing time provided optimal curing conditions resulting in the most desirable mechanical and physical properties. However, toughness was greatly reduced with the increase of the CO_2 pressure, curing time, and rolling pressure. Additionally, the carbonation curing improved the bonding between the fiber and the cement matrix because of the precipitation of calcite particularly in the pores of the interfacial transition zone (ITZ) between the cement matrix and the fibers.

Keywords: fiber-cement composite; mechanical properties; carbonation; parametric study

1. Introduction

Fiber-cement products are nowadays widely used in the world because of their versatility for manufacturing construction materials such as lightweight roof tiles, ceilings, decorative components, and floors, which are used in most houses in developing countries as well as in agricultural and industrial buildings [1,2]. The fiber-cement industry has grown rapidly because of increased demand. As such, the rheological [3,4] and mechanical [5,6] properties of fiber-cement composites have been extensively studied. However, the cement industry is the third-largest source of carbon dioxide emissions. One of the considered strategies to mitigate CO_2 emissions is carbon dioxide capture and storage (CCS) [7]. The current storage methods focus on enhanced oil recovery, underground geological storage, and disposal in deep oceans [8]. Alternatively, optimization of fiber-cement composites by

curing at elevated CO_2 conditions could, on the one hand, enhance the mechanical properties and on the other hand reduce carbon dioxide emissions.

Many researchers point out that the carbonation process offers several benefits including durability improvement, reduction of porosity [9], reduction of the average pore size [10] associated with the increased densification of the matrix through the precipitation of $CaCO_3$, which is a denser and more stable product than $Ca(OH)_2$ [11], and strength gain [12]. Therefore, such a technology can reduce carbon dioxide emission from major point sources while developing a value-added product at the same time. However, the carbonation of cementitious composites leads to a decreased alkalinity of the cement matrix due to a lower portlandite content, which can cause faster corrosion of steel reinforced concrete [13]. The atmospheric CO_2 diffuses into concrete and reacts with calcium hydroxide, the main hydration product of cement, resulting in a decrease of pH, which leads to the initiation of corrosion of steel reinforcement bars (loss of the passivation layer at lower pH). This phenomenon, called passive carbonation of concrete, is a major deterioration mechanism of reinforced concrete structures. Another negative effect is carbonation-induced shrinkage which is sometimes mentioned in the literature [13].

Carbonation processes can be classified into two types: carbonation of hardened cementitious materials, or carbonation curing of fresh cementitious materials in which CO_2 reacts with the anhydrous phases and hydration products to form calcium carbonate [14,15] resulting in a stronger composite [14,16]. Carbonation curing of fresh materials including accelerated CO_2 curing has been considered to be a beneficial and economical process, which offers a possibility to help to reduce the dominant greenhouse gas CO_2 by capturing it in stable carbonate forms, and resulting in enhanced mechanical properties. Among the various cementitious products such as precast, non-reinforced concrete, bricks or concrete products with non-metallic reinforcements [17], and fiber-cement composites that can be used in the accelerated CO_2 curing process, the fiber-cement composites, in particular, are chosen in this study because they do not have any steel bars (which poses a threat for long-term performance). Moreover, the thickness of the fiber-cement products in our case is very thin (4–5 mm), which could increase the carbonation degree as the permeation of CO_2 can be very fast along the depth.

There are a lot of factors influencing the carbonation. The concentration of CO_2 is the dominant factor as the carbonation reaction rate is significantly influenced by the CO_2 concentration. In atmospheric conditions in which the CO_2 concentration level is around 0.03%–0.04%, the rate is slower than in accelerated curing conditions in which the concentration could be up to 100%. In natural conditions, the complete carbonation of engineering sized components takes many years but only a few hours or days under laboratory conditions by increasing the CO_2 concentration, especially in case of application of a pressure gradient to facilitate transport processes and dissolution of CO_2 [14,18]. Controlling surrounding relative humidity (RH) is very important to accelerate the carbonation process. Walton et al. showed that carbonation was more rapid at a relative humidity of 50–70% and decreased at higher and lower relative humidity [19,20]. The increase of temperature (up to 60 °C) increases the CO_2 uptake due to the leaching of Ca^{2+} ions from the solid phases [21]. Finally, the initial conditions of the cementitious materials are also important such as the water to cement ratio, the initial porosity, and density. In this study, we changed the initial physical characteristics of the specimen by changing the rolling pressure during the Hatschek process. The Hatschek process consists of producing fiber-cement sheets by stacking thin laminas made from a suspension of cement, fibers, mineral admixtures, and water.

Consequently, there are many parameters (e.g., CO_2 concentration, temperature, and relative humidity) to be optimized in the accelerated carbonation curing process to obtain a high-performance composite. Only a few studies have been reported in the literature in which accelerated CO_2 curing is considered for fiber-cement composites under different conditions. Almeida et al. [22] studied carbonated cementitious specimens reinforced with bleached eucalyptus pulp, with a climate chamber set to 60 °C temperature, 90% RH, and atmospheric CO_2 concentration (15 vol %) for two days. The results showed that the mechanical properties were better for the composites subjected to accelerated carbonation at early stages of hydration and carbonated samples presented higher values of

mechanical properties for all aging tests (400 accelerated aging cycles and 1 year of natural weathering). For the non-carbonated samples, the highest modulus of rupture (MOR) was found for the samples that were exposed to one year of natural weathering (CO_2 from the atmosphere). Pizzol et al. [23] studied the accelerated carbonation process in cementitious specimens reinforced with bleached cellulosic pulp and synthetic fibers, with the same carbonation conditions as Almeida et al. for ten hours. Even with such a short curing time, the carbonated products exhibited a good fiber–matrix bonding, improved mechanical properties with a reduction of composite degradation. Santos et al. [16] studied the supercritical carbonation of extruded fiber-cement reinforced with bleached eucalyptus pulp and residual sisal chopped fibers, with specimens placed in a chamber with total saturation (close to 100% concentration) of supercritical CO_2 at 20 MPa with the chamber immersed in water at 45 °C. The results showed that the supercritical carbonation treatment for only 2 h could significantly improve the physical characteristics and mechanical performance.

It has been proved that carbonation of fiber-cement composites may improve the interfacial transition zone (ITZ) between cement paste and fiber [24], which significantly enhances the tensile strength of fiber-cement composites. In particular, nanofibrillated cellulose based fiber-cement composites show significantly better mechanical behavior compared to the composites without nanofiber. This improvement is attributed to the better bonding between the nanofibrils and the cement matrix. However, under accelerated aging by carbonation, the composites with or without nanofibers do not reduce the mechanical performance due to the lower alkalinity provided by the accelerated carbonation. Therefore, the nanofibrillated cellulose appears to be a promising material to be used as nano-reinforcement of the extruded hybrid cement-based composites [25]. Moreover, PVA and macro-synthetic fibers offer a good performance in terms of bonding strength with the cement matrix thanks to its hydrophilicity [26,27], which compensates for the potential of cracking occurring in the matrix. Therefore, they are effective in improving durability, including permeability of the matrix [26].

The aim of this paper was to study the influence of the rolling pressure, the CO_2 curing time, and the CO_2 pressure on PVA and cellulose based fiber-cement composites hydrated in semi-adiabatic conditions with high concentration carbonation at an early age. Samples were produced with the Hatschek machine, in the real process of the Mahaphant Fiber-Cement Public Company Limited (Lopburi, Thailand). The samples were subjected to three different sets of rolling pressure during the Hatschek process, three different curing times and two different curing pressures, thus allowing for a comparison between the physical and mechanical properties of samples with and without carbonation under various conditions. In addition, this study also considers linear and non-linear regression analysis of various mechanical and physical parameters in order to optimize the carbonation curing conditions and hence to optimize the performance of fiber-cement composites.

2. Materials and Methods

2.1. Materials and Mix Design

2.1.1. Fiber

Two types of fiber acting as reinforcement were used: cellulose pulp and synthetic PVA fibers. The cellulose fibers are refined at various freeness values depending on the product categories. Refining (also termed beating) fibrillates the surface of the fiber and creates dilute slurries of cellulose fibers to drain more slowly [28]. Freeness values in this study were given as Canadian standard freeness (CSF) values determined according to TAPPI T 227 om-04: freeness of pulp [28,29]. The cellulose fibers with 160-level freeness, 30-micron diameter, and 1.8-mm average length, and the synthetic PVA fiber with 14-μm diameter and 4-mm length were used in this study. Morphological properties of the cellulose fiber are presented in Table 1.

Table 1. Morphological properties of the cellulose fiber.

Properties	Elastic Modulus	Tensile Index	Tear Index	Freeness
	(MPa)	(N m/g)	(mN m2/g)	(-)
Cellulose fiber	10837	58.18	11.17	160

2.1.2. Cement

The cement used in this study was ordinary Portland cement (OPC) in accordance with ASTM C 150, Type I [30] (INSEE Petch Portland cement type I in Thailand, which is equivalent to OPC CEM I 42.5 N according to European Standard EN197-1). This cement was used because of its fine particle size and high compressive strength ($\geq$33 MPa and 42 MPa at 7 and 28 days, respectively). Chemical compositions of the cement and ground limestone (shown in the next subsection) were determined using X-ray fluorescence spectrometry and are presented in Table 2.

Table 2. Chemical composition of cement and limestone (% by mass of oxide).

% Oxide	CaO	MgO	SiO$_2$	Al$_2$O$_3$	Fe$_2$O$_3$	K$_2$O	SO$_3$	P$_2$O$_5$	TiO$_2$
Portland cement	62.70	0.85	20.01	4.41	3.48	0.37	2.73	0.07	0.25
Limestone	91.12	2.42	1.52	0.56	0.24	0.16	-	-	0.1

2.1.3. Limestone Filler

The filler used in this study was pulverized limestone. This filler was used for partial substitution of Portland cement to reduce the cement consumption, hydration heat, and promote particle packing resulting in a robust dimensional stability [31]. Furthermore, limestone filler also acts as a nucleation side for calcium carbonate precipitation which enhances the carbonation degree [9].

### 2.1.4. Fiber-Cement Composite Mix Design

The dry mixture (by weight percentage) consisted of 75% OPC type I cement, 20% limestone filler, 3% cellulose fiber, and 1% synthetic fiber (PVA). The water to cement ratio was initially controlled at 0.62 (after passing the Hatschek machine which was initially designed by Shera Public Company (Bangkok, Thailand) This proportion of fiber content was well-suited for the production method used (a crude reproduction of the Hatschek industrial method), which allowed the inclusion of a significant amount of fiber in the matrix [22].

Using the Hatschek process, fiber reinforced cement pads with dimensions of 2 m in width and 2 m in length were produced. For the laboratory experiments, the pads were cut into small specimens with dimensions 102 mm $\times$ 210 mm $\times$ 5 mm. These dimensions were necessary for the samples to fit into the available carbonation chamber.

2.2. Setup

2.2.1. Accelerated Carbonation Apparatus

The machine (Figure 1) was comprised of a series of pressure valves and a pump to inject CO$_2$ into a steel chamber, which contained 15 samples. Carbon dioxide with approximately 99.5% purity was injected into the chamber. The CO$_2$ used in the experiments was supplied by the Linde Thailand Company (Samutprakarn, Thailand). The pressure was regulated between 1 to 3 bars using a system of seals and gaskets.
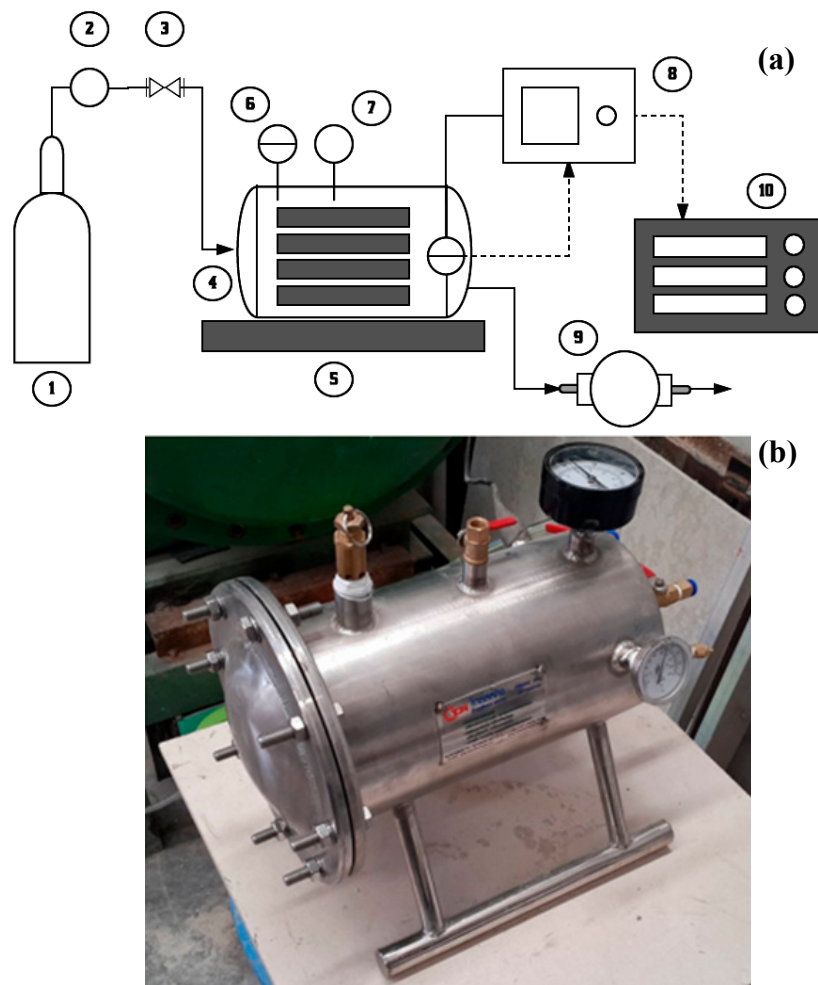
Figure 1. A Schematic setup (**a**) and a photo (**b**) of the accelerated carbonation apparatus: 1. CO_2 gas tank; 2. Flow transmitter; 3. Pressure regulator; 4. Curing chamber; 5. Digital scale; 6. Pressure gauge; 7. Temperature gauge; 8. CO_2 and humidity sensor; 9. Vacuum pump; 10. Data logger.

2.2.2. Rolling Pressure of the Hatschek Machine

The pads were made using a slurry-dewatering process followed by a pressing technique, a simplified reproduction of the Hatschek process used in the industrial production of fiber-cement [12]. The rolling pressure is an important parameter to control the water to binder ratio [32]. In this study, the rolling pressure was varied between 2.5 to 9 bars to study the impact on the physical and mechanical properties of the samples.

2.2.3. Composite Preparation and Curing

Fiber-cement pads were exposed to two different curing conditions:

(a) Non-Carbonated Curing (NCC): The samples were placed into a chamber with semi-adiabatic conditions for 8 h. Following this step, the samples were maintained in air saturated curing (i.e., sealed in plastic bags) under 25 °C until they attained an age of 3, 7, 14, and 28 days. These samples are identified as non-carbonated composites in this work.

(b) Accelerated Carbonation Curing (ACC): The samples were placed into a chamber with semi-adiabatic conditions for 3, 5, and 9 h at different CO_2 pressures (1 and 3 bar). After that, they were kept in air saturated curing (i.e., sealed in plastic bags) under 25 °C until 3, 7, 14, and 28 days of age. These samples are referred to as carbonated composites.

Curing was carried out under semi-adiabatic conditions in order to accelerate the hydration reactions and uptake of CO_2, in which the temperature increased up to 60 °C (shown later in Section 3.1).

2.3. Characterizing Physical Properties of Fiber-Cement Composites

Apparent void volume (AVV), bulk density (BD), and water absorption (WA) of the composites were obtained from the average of five test specimens (160 mm × 25 mm × 5 mm) for each condition, following the procedures specified by ASTM C 948–81 [33]. Physical properties were obtained using Equations (1)–(3):

$$\text{AVV}(\%) = \left(\frac{W_{\text{sat}} - W_{\text{dry}}}{W_{\text{sat}} - W_{\text{i}}} \right) \times 100 \tag{1}$$

$$\text{BD}\left(\text{g/cm}^3\right) = \left(\frac{W_{\text{dry}}}{W_{\text{sat}} - W_{\text{i}}} \right) \times \rho \tag{2}$$

$$\text{WA}(\%) = \left(\frac{W_{\text{sat}} - W_{\text{dry}}}{W_{\text{dry}}} \right) \times 100\% \tag{3}$$

where W_{sat} (g) is the saturated weight of the sample with a dry surface measured after 24 h immersion in water, W_{dry} (g) is the dry sample weight after 24 h at 105 °C, W_{i} (g) is the weight of sample immersed in water, and ρ (g/cm^3) is the density of water.

The carbonation depth of the cement matrix was observed by spraying a solution of phenolphthalein onto the freshly broken surfaces, i.e., the cross-section of the samples, which is commonly used as an indicator of the pH [34–36]. This solution is purple when reacting with alkaline substances and is colorless in the presence of acid substances, indicating the extent of the carbonation reaction in the cement matrix because of the lower $Ca(OH)_2$ content that decreases the pH. In our case, the phenolphthalein spraying was only performed on the outer and fracture surfaces of the carbonated samples at an age of 28 days. Therefore, we could only observe change in color on the surface of the samples. This is because, after carbonation, the hydration continued resulting in a high pH pore solution again. Therefore, we still observed a pink color of the fractured samples when exposed to phenolphthalein solution. A new set of samples have now been carbonated again and the carbonated depth will be measured right after carbonation (results will be shown in a forthcoming paper).

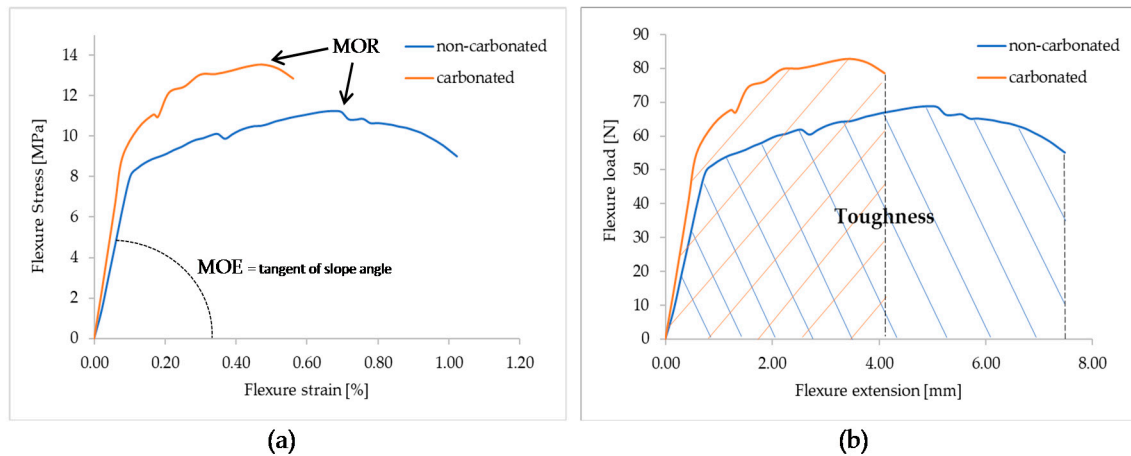### 2.4. Characterizing Mechanical Properties of Fiber-Cement Composites

Mechanical properties were obtained for NCC and ACC after 3, 7, 14, and 28 days. Five samples were evaluated for each condition (i.e., duration). These results were calculated based on the 3-point bending test described in ASTM Standard C 1185 with a universal testing machine Instron 3300. The samples were loaded at a rate of 12.7 mm/min to achieve failure within 5 and 30 s according to the ASTM method Standard C 1185. The exception is that the samples had dimensions of 102 mm in width and 210 mm in length because of the limitation of our laboratory. The test span was 200 mm. The Modulus of Elasticity (MOE) was determined from bending experiments and in accordance with Equation (4) (see Figure 2a). The flexural toughness was calculated as the area under the load/displacement curve up to the point of failure as presented in Figure 2b and in accordance with Equation (5). The point of failure is nothing but the Modulus of Rupture (MOR), also known as the flexural strength, determined in accordance with Equation (6). The flexural toughness (sometimes called fracture toughness (kJ/m^2)) is actually the energy (E, (kJ)) absorbed during the bending test divided by the cross-sectional area of the specimen and obtained by integrating the load vs. deflection curve up to the point, which corresponds to a reduction in the load carrying a capacity of 30% of the maximum load [37].

$$\text{MOR (MPa)} = \frac{3 \cdot P_{max} \cdot L_v}{2 \cdot b \cdot h^2} \tag{4}$$

$$\text{MOE (MPa)} = \frac{m \cdot L_v^3}{4 \cdot b \cdot h^3} \tag{5}$$

$$\text{Toughness}\left(\text{kJ}/m^2\right) = E / \left(b \cdot h \cdot 10^{-6}\right) \tag{6}$$

where P_{max} (N) is the maximum load, L_v (mm) is the support span length, b (mm) and h (mm) are the specimen width and depth respectively and m (N/mm) is the tangent of the slope angle of the load vs. deflection in the elastic range [22,38].

(a)   (b)

Figure 2. The flexural stress versus flexural strain/deflection curves to characterize the mechanical properties of the cement composite materials: (**a**) Modulus of rupture (MOR) and modulus of elasticity (MOE); (**b**) toughness.

2.5. Microstructural Analysis Using Scanning Electron Microscopy

The effect of the early-stage accelerated carbonation curing on the fracture surfaces resulting from the mechanical tests at 28 days was analyzed using scanning electron microscopy with a secondary electron (SE) image detector, operated at 20.0 kV accelerating voltage, for visualization of the microstructure on the fractured surface of the composites. Fractured surfaces were gold coated with a Bal-Tec SCD050 coating system before being analyzed in a Zeiss LEO Evo 40 microscope. The images magnifications used ranged 5000×.

3. Results and Discussion

3.1. Effect of Curing Time on Mechanical and Physical Behavior

Figure 3 shows the relationship between the mechanical properties (MOR, MOE, and toughness) and carbonation curing period. In general, the increase of curing time considerably improved the mechanical properties of the carbonated cementitious matrix. Different mechanical behavior was found for the carbonated composites with increased carbonation time (Figure 3). The carbonated composites at any curing period showed higher average values of MOE and lower toughness than non-carbonated ones. However, only the long curing period of 9 h exhibited higher MOR, with similar values for 5 h curing and even lower MOR for 3 h curing. Figure 3 also shows an increase in MOR and MOE and decrease in toughness due to continuous hydration up to 28 days.

For MOR, the carbonated composites indicated a better mechanical performance at 28-day testing, with approximately 2.4% and 6.4% increase after 5 h and 9 h curing time, respectively, compared to the non-carbonated samples. These beneficial outcomes would have resulted from the lower fiber deterioration under the less matrix alkalinity, which helped improve the fiber-matrix bond-ability and allow the dissipation of energy in the post-cracking region. However, MOR was slightly decreased at a shorter carbonation curing time (3 h) because the temperature during curing sharply dropped when

removing the sample from the curing chamber. The rate of hydration and hence also the carbonation reaction rate decreased compared to the reference samples cured under semi-adiabatic conditions up to 8 h, while at longer curing time, the degree of hydration and carbonation reaction were much higher compared to that at 3 h curing.
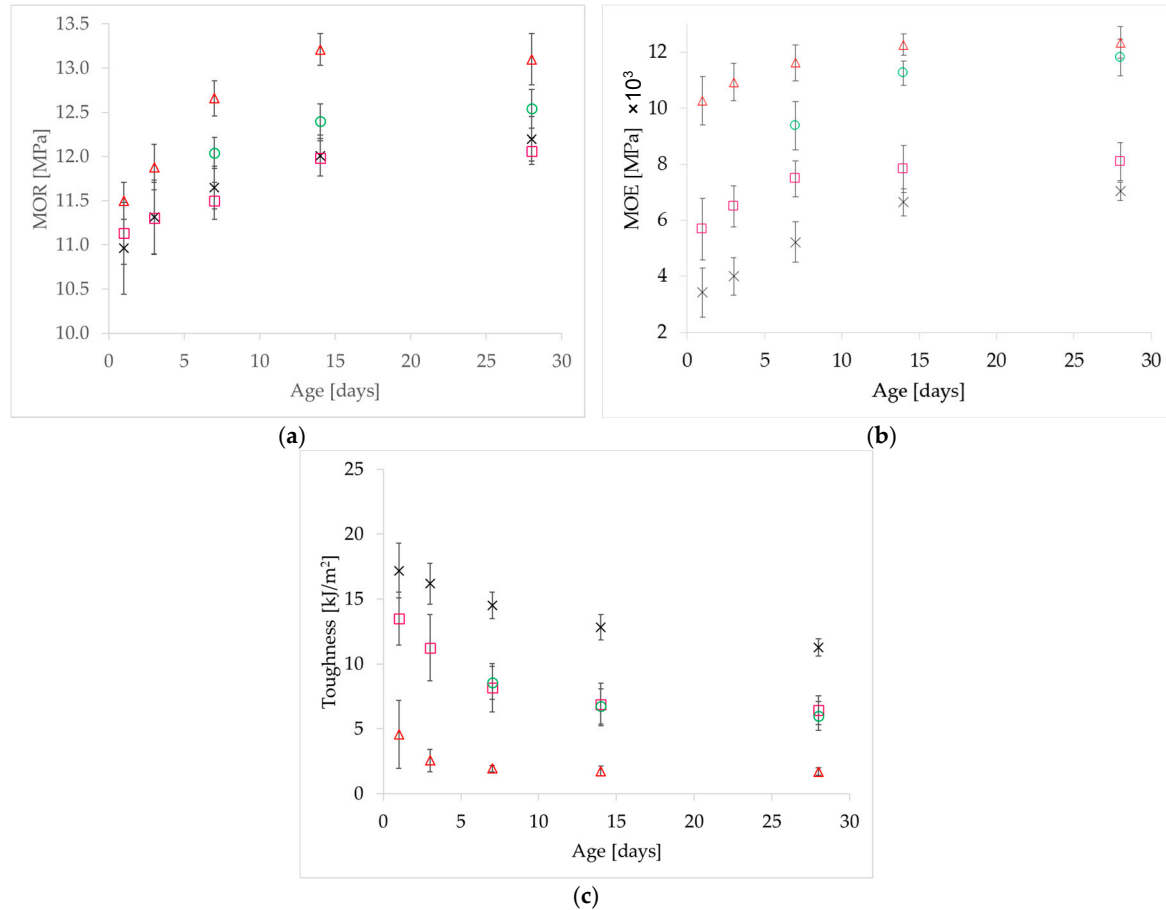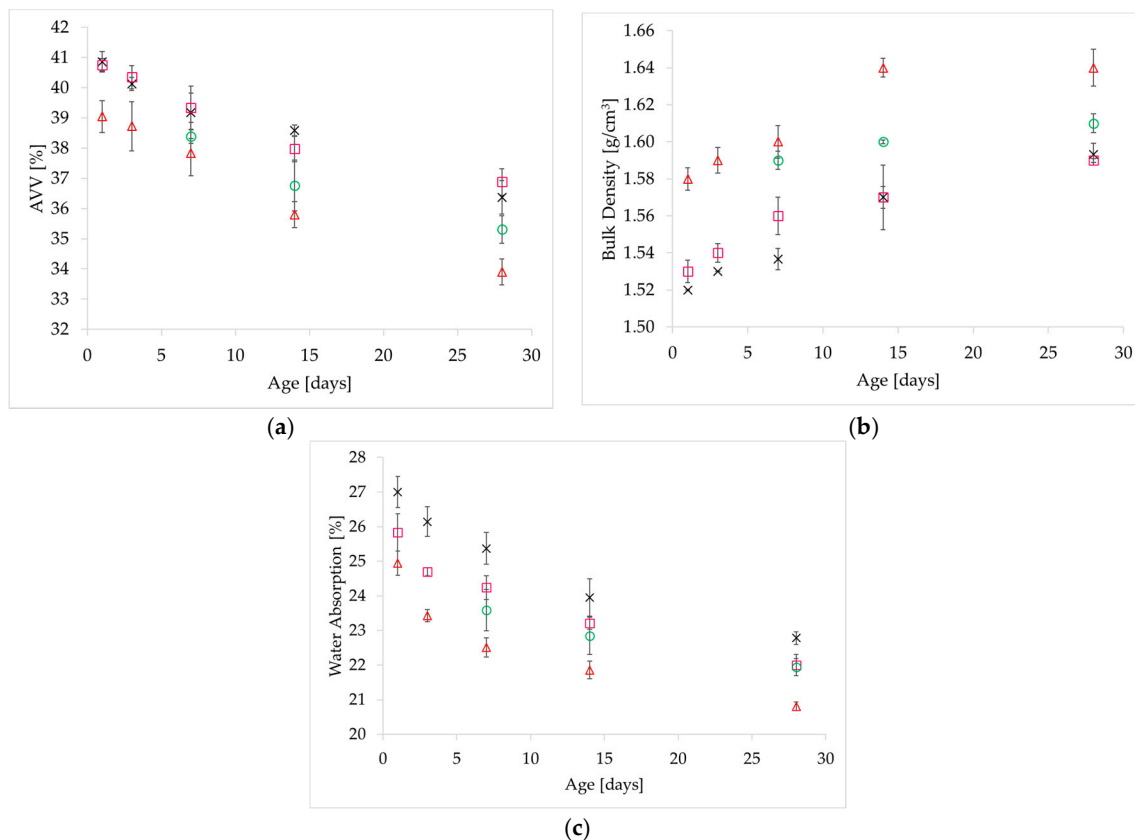

Figure 3. Average values of mechanical properties at different carbonation time (×non-carbonated curing (NCC), □ 3 h accelerated carbonation curing (ACC), ●5 h ACC and Δ 9 h ACC): (**a**) Modulus of rupture (MOR); (**b**) modulus of elasticity (MOE) and (**c**) toughness.

The MOE was significantly increased by 15.6%, 66.5%, and 76.5% for 3, 5, and 9 h carbonation time, respectively. This behavior is attributed to the reactions taking place during carbonation in which there was precipitation of calcium carbonate ($CaCO_3$) in the pores [39], especially on the surface. The calcium carbonate densified the matrix and improved the fiber-matrix bond (i.e., ITZ) and consequently the mechanical behavior of the fiber-cement composite [14,22]. Note that even at a short curing period (3 h), the MOE still increased despite the decrease of MOR because the slope of the stress-strain curve (see Figure 2) was still increased compared to the reference samples, while the strength could be lower resulting in lower MOR (see Equation (5)).

The flexural toughness values were lower for the carbonated samples (Figure 3c), an approximate decrease of 38.7%, 48.7% and 85.3% for 3, 5, and 9 h carbonation time, respectively. The results show that the toughness was negatively correlated with carbonation time, the longer carbonation time, the lower the toughness. Reduction of toughness can be compensated for by the increase of MOE, but should not be less than, 5 kJ/m^2, which is the minimum value required for proper transportation and installation of cement fiber composites at the construction site.

Figure 4 shows the comparison of the effects of the accelerated carbonation on the physical characteristics of water absorption, apparent void volume, and bulk density for carbonated and noncarbonated fiber-cement composites at different carbonation times. The results demonstrated that accelerated carbonation is effective in improving the physical properties because of pore filling with carbonate products resulting in a decrease of apparent void volume (AVV) by 2.9% and 6.5%, a decrease of water absorption (WA) by 4.2% and 9%, and an increase of bulk density (BD) by 1.2% and 2.5% after 5 and 9 h carbonation time at 28 days, respectively. This is again the consequence of the increase of $CaCO_3$ in the composites, which reduces the porosity due to the higher molar volume of $CaCO_3$ compared to $Ca(OH)_2$—the main carbonated phase in the cementitious matrix [40]. However, it was noticed that the precipitation of $CaCO_3$ crystals has a negative role on the carbonation degree due to pore clogging. The porosity decrease (represented by AVV in this study) and bulk density increase have also been observed by many researchers such as in the study of Silva et al. [41], who showed a reduction of 15% in porosity and approximately 6.5% increase in the bulk density of the composites subjected to accelerated carbonation for 14 days.

(a)

(b)

(c)

Figure 4. Average values of physical properties with different carbonation time (× NCC, □ 3 h ACC, ●5 h ACC and Δ 9 h ACC): (**a**) Apparent void volume (AVV); (**b**) bulk density (BD) and (**c**) water absorption (WA).

The bulk density evolution (*W*, calculated as relative weight change in %) provides a quantitative estimation of the amount of CO_2 uptake during carbonation. The weight increase in this study was 1.2% and 2.5% (as shown earlier) after 5 and 9 h carbonation under semi-adiabatic conditions, respectively. If only portlandite is carbonated, we can estimate the CO_2 uptake as follows:

$$Ca(OH)_2 + CO_2 \rightarrow CaCO_3 + H_2O \tag{7}$$

$$\text{Uptake}_{CO_2} = \left(\frac{M_{CO_2}}{M_{CaCO_3} - M_{Ca(OH)_2}} \right) \times W \tag{8}$$

where M_{CO_2}, M_{CaCO_3}, and $M_{Ca(OH)_2}$ (g/mol) denote the molar weight of CO_2, $CaCO_3$, and $Ca(OH)_2$, respectively. The CO_2 uptake is then 2.0% and 4.2% for 5 and 9 h carbonation curing, respectively. Pizzol et al. [23] showed that the CO_2 uptake in the composites subjected to 4 h and 10 h of accelerated carbonation in a climate chamber at around 60 °C and 90% relative humidity (RH) was 10% (equivalent to around 0.5 kg of CO_2 uptake/m^2 roof with 4 mm thickness) and 18% (equivalent to around 0.8 kg of CO_2 uptake/m^2 roof with 4 mm thickness), respectively. Those results are higher than our results because of the fact that they carbonated the samples at higher initial temperature and the RH in the chamber was maintained at 90%, while in our case, the temperature started at 25 °C and increased up to a maximum temperature of 60 °C in 3 h (as seen in Figure 5) and the RH may be much higher than 90% as water accumulated in the chamber during carbonation. Therefore, higher temperature could accelerate the hydration and carbonation, while lower RH could induce faster carbonation. Furthermore, our estimation does not take into account the carbonation of C-S-H [10] and other minor phases, which could result in an underestimation of CO_2 uptake.

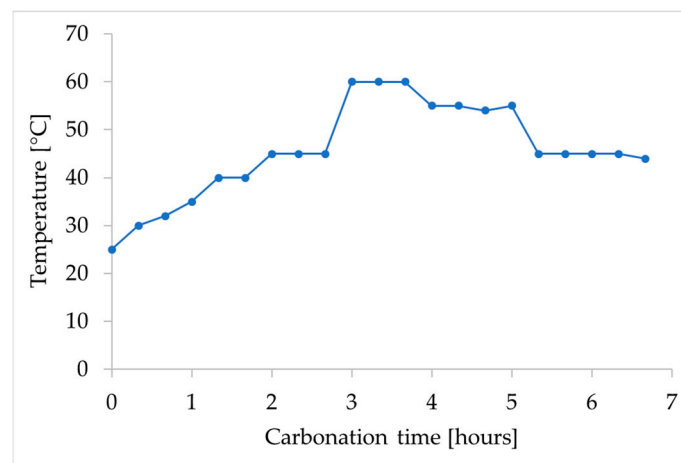**Figure 5.** Temperature profile in carbonation chamber at 3 bar CO_2 pressure.

3.2. Effect of CO_2 Pressure on Mechanical and Physical Behavior

The effects of applied CO_2 pressure on carbonation are shown in Figure 6. When pressure was increased from 1 to 3 bar at 28 days, MOR increased from 11.3 to 13.1 MPa and MOE increased from 10,053 to 12,342 MPa for 9 h curing time. On the other hand, the pressure increase caused a negative impact on the toughness, which was reduced from 3.48 to 1.71 kJ/m^2 for 9 h curing period and a smaller reduction for a shorter curing period. In the case of 1 bar, the carbonation was very limited when cured for less than 5 h because of low pressure. Furthermore, when the samples were retrieved from the chamber after carbonation, heat loss occurred. Therefore, the curing temperature was less than for the case of non-carbonated samples, which compensates the slight MOR gain because of carbonation. Therefore we observed similar MOR for both carbonated and non-carbonated samples. However, the results showed that there were some differences in mechanical properties of 5 and 9 h carbonation and if we increase the carbonation time up to 1 day or more, the improvement of MOR would be clearer as shown in [42].

Higher CO_2 pressure also improved the physical properties as shown in Figure 7. AVV decreased from 34.9% to 33.9% when CO_2 pressure was increased from 1 to 3 bar in the case of 9 h carbonation curing. The same observation was made for the WA, whose value decreased from 21.82% to 20.81%, while the BD increased from 1.60 to 1.64 g/cm^3.

(a)

(b)

(c)
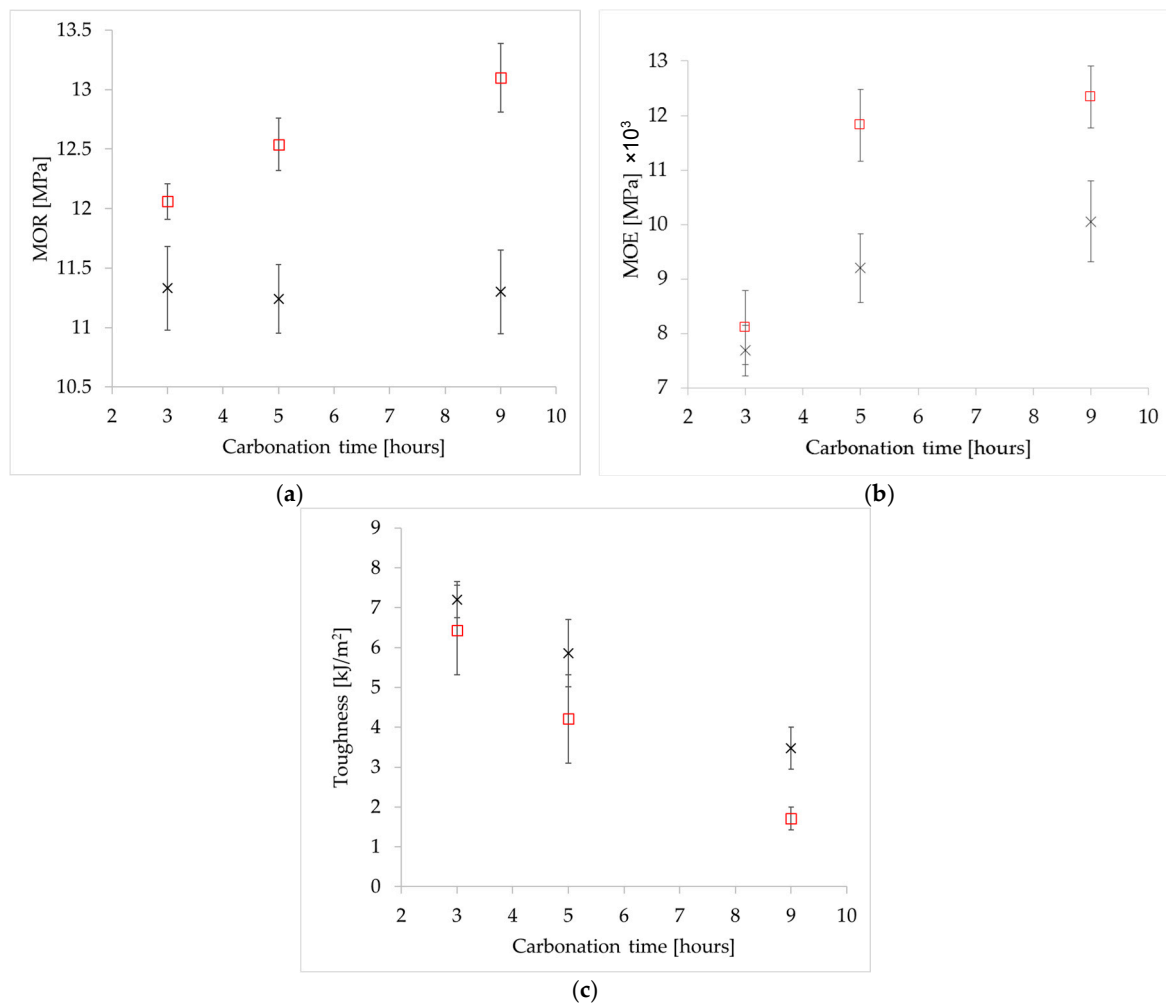
Figure 6. Average values of mechanical properties at different CO_2 pressures ($\times$ 1 and $\square$ 3 bar CO_2 pressure): (**a**) Modulus of rupture (MOR); (**b**) modulus of elasticity (MOE) and (**c**) toughness.

(a)

(b)

Figure 7. *Cont.*

(**c**)
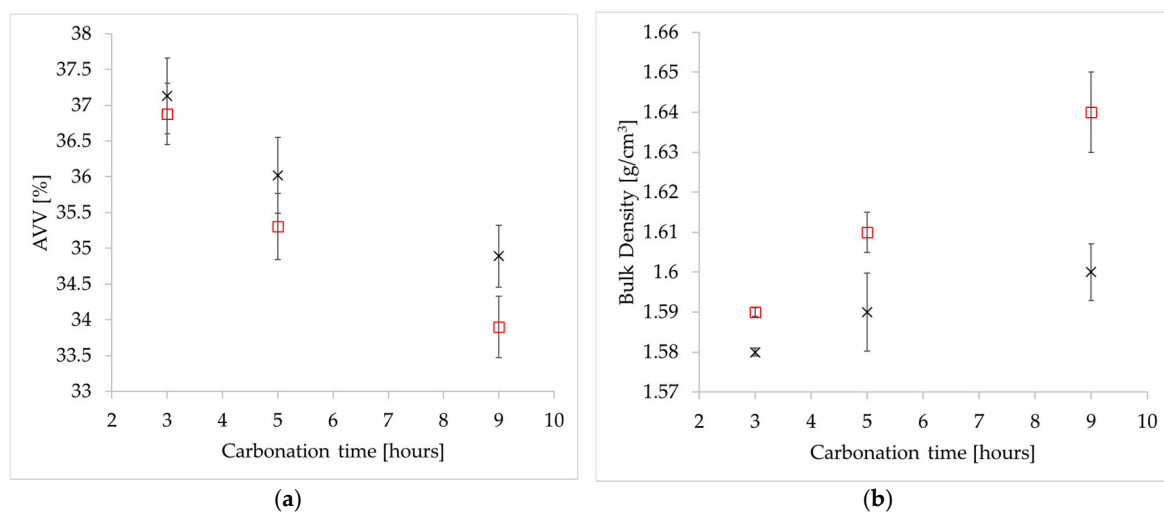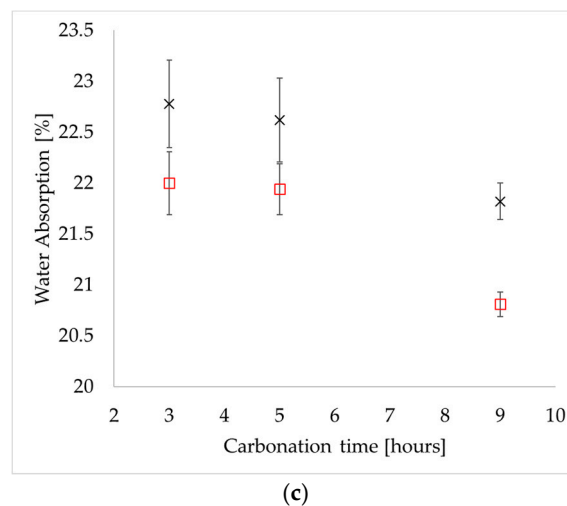
Figure 7. Average values of physical properties in difference CO_2 pressure ($\times$ 1 bar and $\square$ 3 bar CO_2 pressure): (**a**) Apparent void volume (AVV); (**b**) bulk density (BD) and (**c**) water absorption (WA).

Higher CO_2 pressure increases CO_2 penetration into the samples [40] resulting in improved physical and mechanical properties. This is because the dissolved CO_2 concentration is related to the gas (CO_2) pressure by Henry's law [43], which means that higher pressure increases the dissolution rate of CO_2 in the pore water of the samples. Furthermore, as long as the sample is not fully saturated, at higher applied pressure, the advective transport (together with advection induced by capillary pressure) contributes to a faster penetration of CO_2 into the samples, and thereby a higher carbonation rate.

3.3. Effect of Rolling Pressure in the Production Process

As stated earlier, this parameter controls the water content in cement-fiber composites. Higher rolling pressure will decrease the water to cement ratio affecting the degree of hydration, which is the main factor influencing the initial microstructure of the cement-fiber composites before carbonation. As such, the carbonation process will behave differently resulting in different evolution of mechanical and also physical properties as seen in Figures 8 and 9. For non-carbonated samples, the results show that, at a high rolling pressure of 9 bar, the MOR and MOE increased up to 13.2 MPa and 12,683 MPa, respectively. However, the toughness decreased from 12.2 to 3.1 kJ/m^2 when the rolling pressure increased from 2.5 to 9 bar. The AVV and WA also exhibited a relative decrease with the increase of rolling pressure, while the BD increased significantly because of water loss at higher rolling pressure.

When the samples were carbonated at a high rolling pressure, the mechanical properties were not significantly affected compared to the non-carbonated samples, except for the MOR, which exhibited a significant increase because of carbonation. In general, when applying higher rolling pressure, the initial pore volume is reduced resulting in a slower CO_2 penetration, thereby lower carbonation degree. This makes the changes in MOE and toughness at a higher rolling pressure much smaller compared to the case with a lower rolling pressure. In this instance, MOE increased by 72.3% at 3 bar of rolling pressure. However, at a higher rolling pressure of 9 bar, the MOE increase was only 9.8% compared to the non-carbonated samples. On the downside, a high rolling pressure can induce cracks in the composites. Therefore, we observed a maximum MOR at 5 bar rolling pressure. With further increase in pressure, cracks could occur and thus a lower MOR. When samples were carbonated, these cracks could accelerate the CO_2 penetration, which results in an increase of MOR. Despite this beneficial effect, the MOR of carbonated samples at 9 bar rolling pressure was still smaller than at 5 bar rolling pressure.
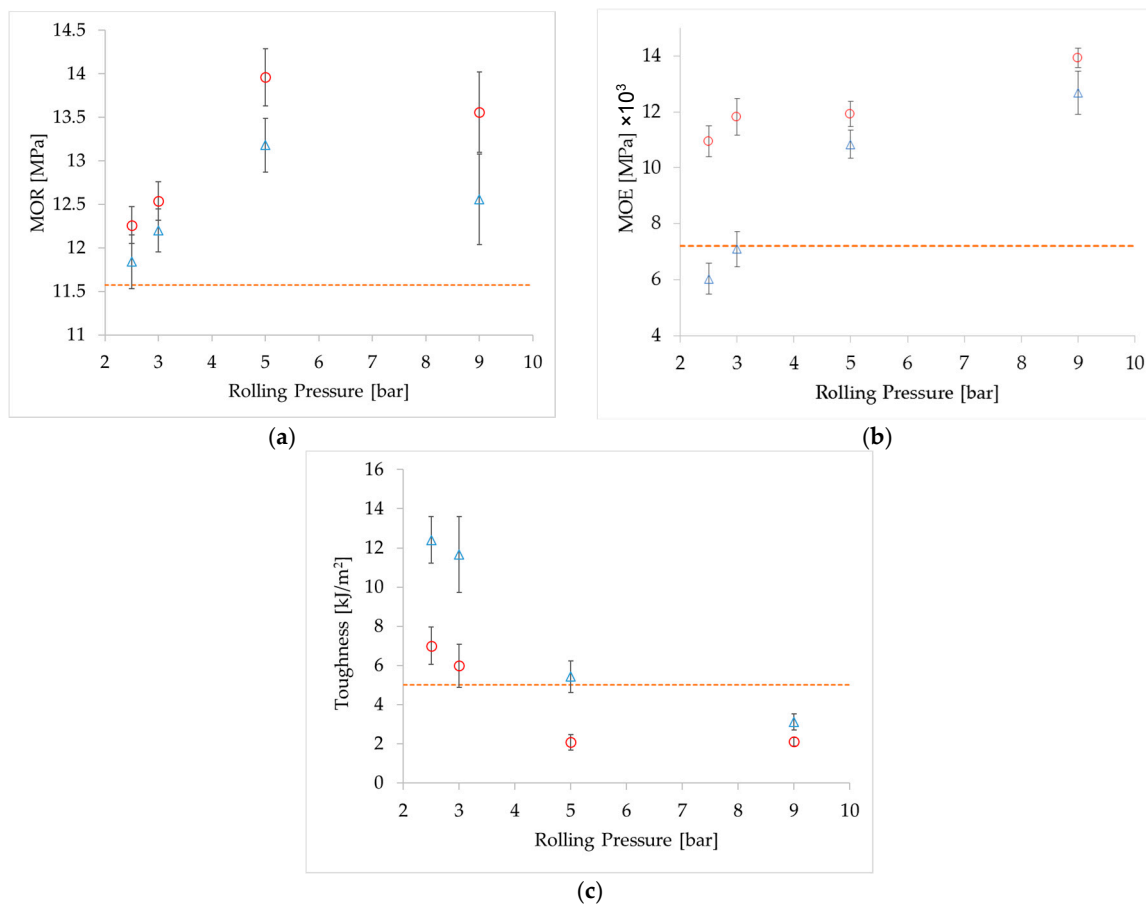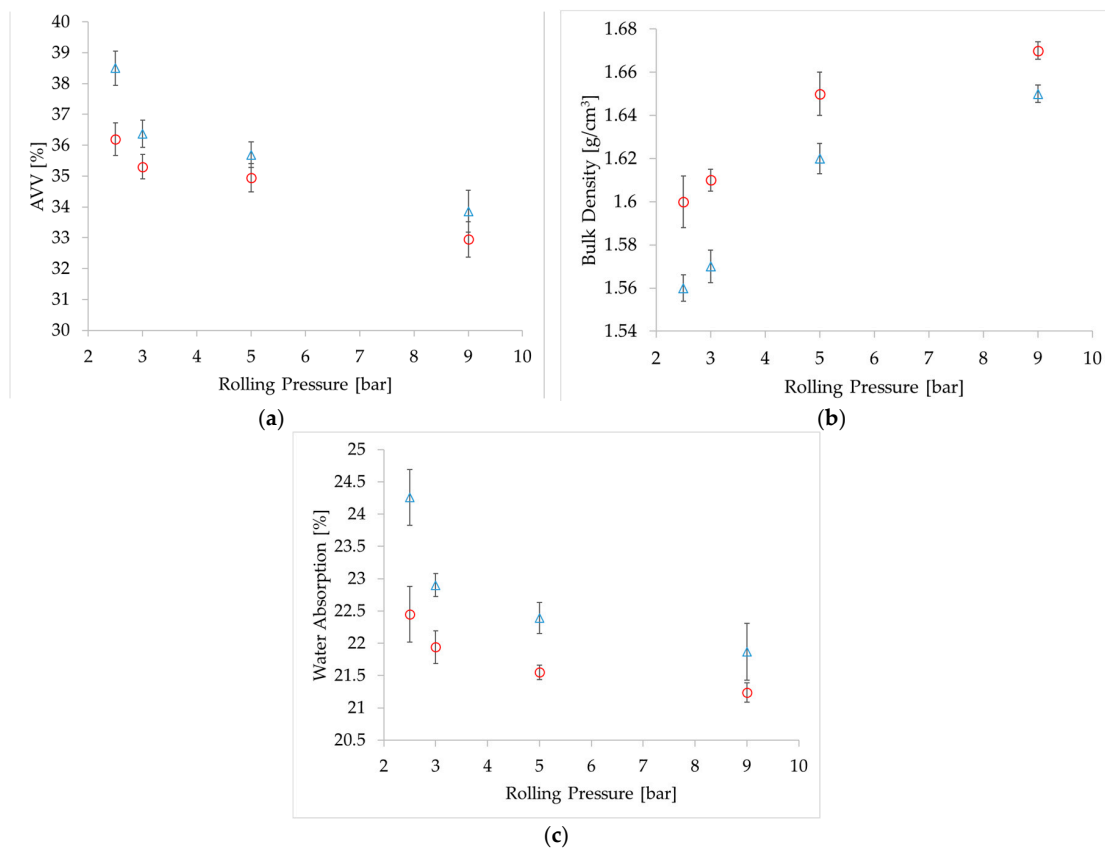
Figure 8. Average values of mechanical properties of non-carbonated and carbonated samples with different rolling pressures (Δ NCC, ●5 h ACC, dotted lines represent minimum requirements): (**a**) Modulus of rupture (MOR); (**b**) modulus of elasticity (MOE) and (**c**) toughness.

Water plays an important role in the carbonation process as carbonation does not occur without water because of its role as a catalyst in the carbonation reaction. However, water can fill the pores and prevent CO_2 gas penetrating into the fiber-cement pore network. In fact, carbonation reaches the highest efficiency at an internal relative humidity close to 60–70% [9], which could never be reached in our case because it requires a much higher rolling pressure that may induce cracks in the composites as discussed above. Therefore, the samples should have low water content but remain uncracked and have a reasonable pore volume to optimize the carbonation process.

Figure 8 also shows the minimum requirements of MOR, MOE, and toughness for fiber cement roof covering products [44]. We can see that whatever the rolling pressure, the MOR and MOE always meet the requirements. However, the toughness is lower than the required value if the rolling pressure is larger than 4 bar. In this sense, the optimal rolling pressure for carbonation curing would be in the range 2.5–3 bar because high rolling pressure may induce cracks resulting in an MOR drop as shown in the case of 9 bar rolling pressure.

The rolling pressure significantly affected the physical behavior of the fiber-cement composites, including AVV, BD, and WA as seen in Figure 9. In general, for both carbonated and non-carbonated samples, a higher rolling pressure reduced AVV and WA and increased BD. When the rolling pressure increased from 2.5 to 9 bar, the average AVV showed a significant decrease of 12% and 9% for non-carbonated and carbonated samples, respectively. This in turn induced an increase in BD by 5% and 4% for non-carbonated and carbonated samples, respectively. As a result, WA dropped significantly, especially for non-carbonated samples by 10%, while recording only 5% decrease for carbonated samples. The changes in AVV, BD, and WA because of carbonation (compared to non-carbonated

samples) were less significant at higher rolling pressure because the higher the rolling pressure the denser the samples, which resulted in a slow CO_2 transport as explained earlier. Consequently, the carbonation degree was lower and had less impact on the physical properties.


Figure 9. Average values of physical properties of non-carbonated and carbonation curing with different rolling pressure (Δ NCC, ●5 h ACC): (**a**) Apparent void volume (AVV); (**b**) bulk density (BD) and (**c**) water absorption (WA).

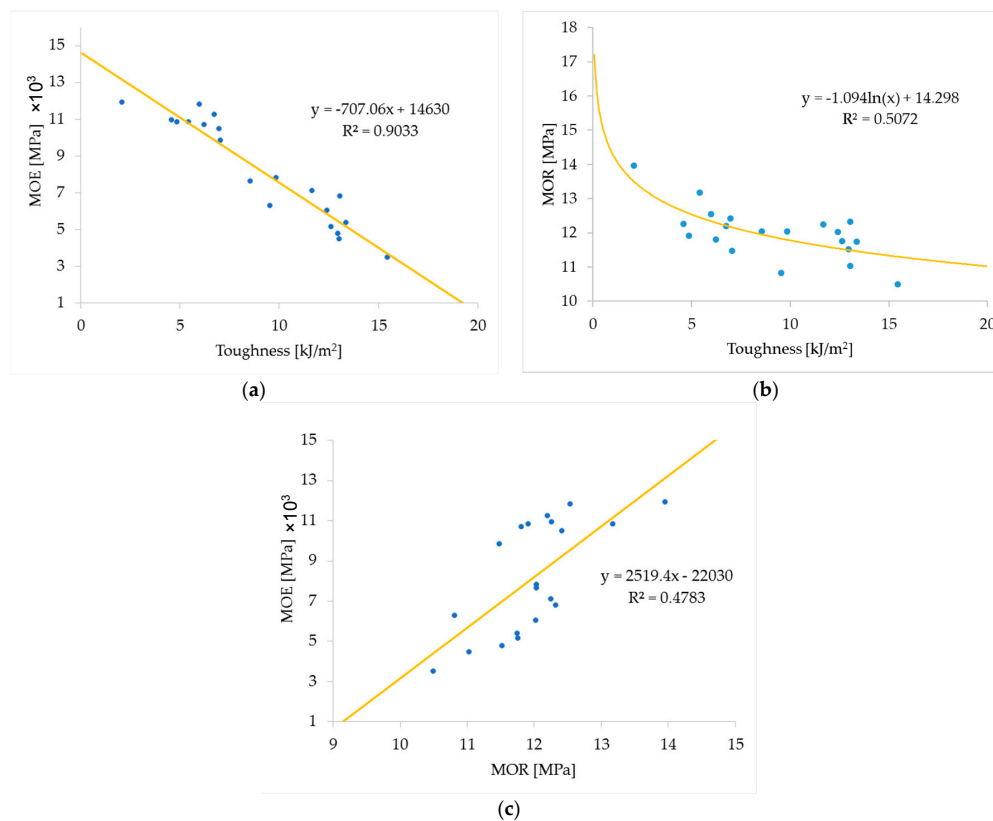### 3.4. Relationship between Modulus of Elasticity, Toughness and Apparent Void Volume

In this sub-section, we try to relate the AVV with MOR and MOE. We used the Ryshkewitch's model, which is widely used for describing the relationship of mechanical properties of porous materials as a function of the solid fraction (equal to 1—air void fraction) [45]. It can be seen in Figure 10a,b that the experimental results are generally in good agreement with the models, with the correlation factors, R^2, being higher than 0.8 for both MOE and MOR. Figure 10c shows that the toughness is increased with the increase of AVV. However, the correlation is not good, with an R^2 of 0.51 for a linear relationship. The toughness is not only affected by AVV but also depends on the loading rate and interfacial zone between the fiber and matrix. Therefore, the uncertainty in measuring toughness is quite high as shown in Figures 3c and 6c, which may partially contribute to the poor correlation. In fact, AVV is not directly linked to the toughness, instead other factors such as MOE have a better correlation (shown later in Figure 11a).

In Figure 11a, we explore the role of MOE to understand how it influences the toughness. In the literature [46], a simple linear regression has become one of the most widely used analytical models for describing the relationship between the MOE and toughness. The results showed a good agreement between the model and experiment data. This agreement is expected because of the fact that toughness can be obtained by integrating the load vs. deflection curve, therefore, the slope or MOE has a major effect on the toughness as shown previously in Figure 2b.
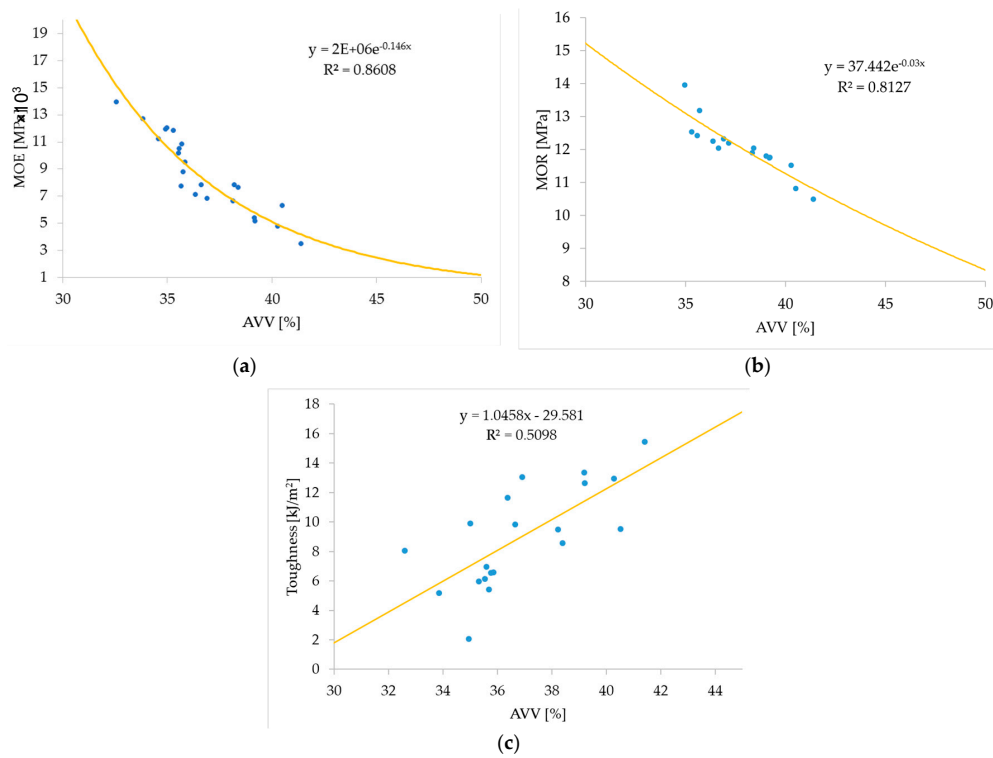
Figure 10. Relationship between mechanical properties and apparent void volume (AVV): (**a**) MOE; (**b**) MOR; and (**c**) toughness.


Figure 11. Relationship between modulus of elasticity (MOE), modulus of rupture (MOR), and toughness: MOE vs. toughness (**a**); MOR vs. toughness (**b**); MOE vs. MOR (**c**).

Figure 11b shows that MOR is significantly reduced with the increase of toughness up to 5 kJ/m^2. With further increase in toughness, MOR slightly decreases. This can be the reason why the required value for toughness is set at a minimum of 5 kJ/m^2. The best fit with experimental data of MOR and toughness is a logarithmic model, despite that the correlation factor is poor (R^2 = 0.51). The MOE also linearly increases with an increase of MOR, but again the correlation is rather poor (R^2 = 0.47) as shown in Figure 11c.

3.5. Evaluation of the Changes in the Microstructure

Micrographs shown in Figures 12 and 13 were obtained by SEM (in secondary electron mode) for the surface and fracture (perpendicular to the surface) of carbonated samples at 1 h and 9 h carbonation curing and also for reference samples. The samples were prepared at the age of 28 days. The analysis of these micrographs allows the observation of the cement phase development and the impact of carbonation on the interface between the fibers and cement matrix. For the surface of the non-carbonated samples, Figure 12a shows needle shaped ettringite (Arrow 1) and small sized CaCO$_3$ around the matrix pores (Arrow 2). Figure 12b shows large sized CaCO$_3$ (Arrow 3), which decreased the AVV of the sample. The ettringite was not observed either in 1 h or 9 h carbonation samples (Figure 12b,c), which suggests that the ettringite was entirely carbonated under accelerated conditions to form CaCO$_3$ phase. Furthermore, we observed that the structure of 9 h carbonated composites was much denser compared to 1 h carbonated samples.

(a)

(b)

(c)
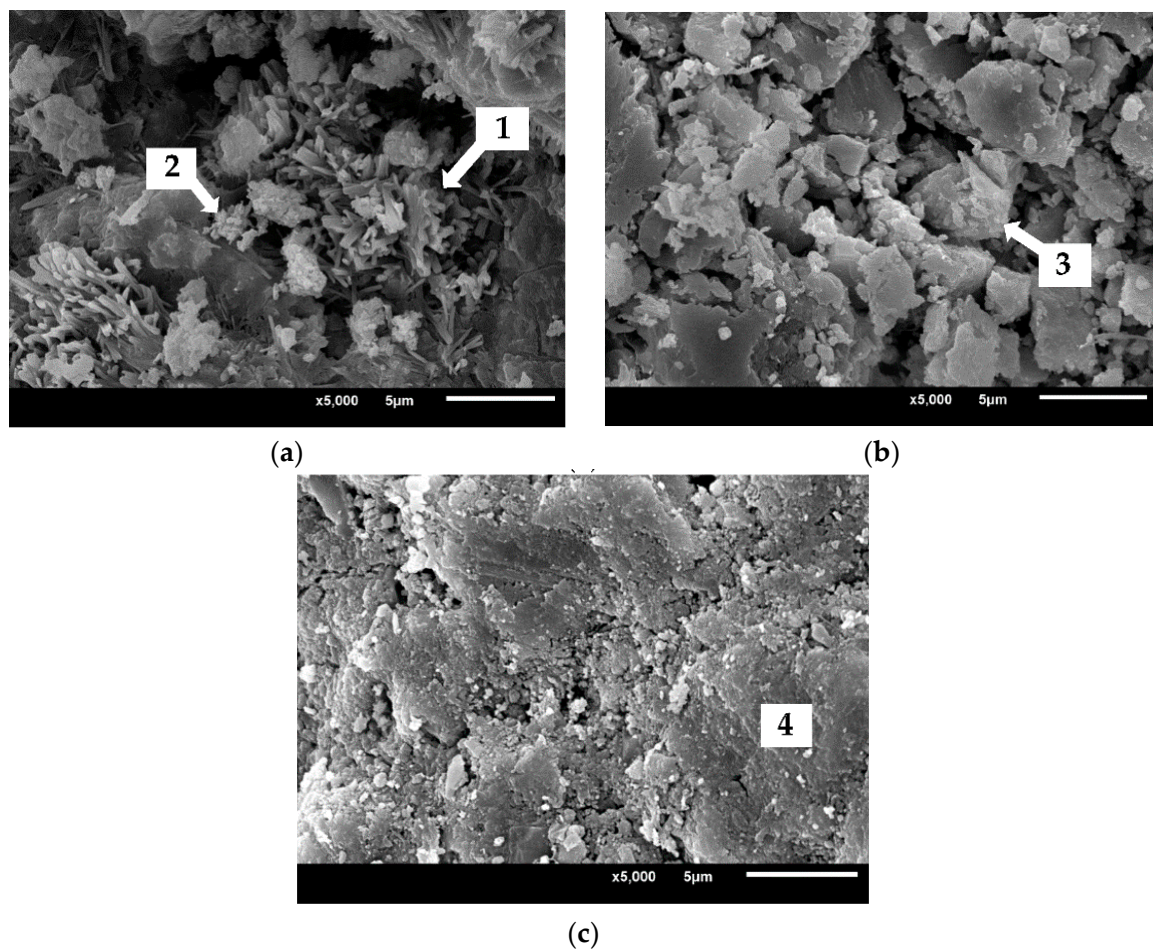
Figure 12. Scanning electron micrographs on the surface of fiber-cement composites: (**a**) non-carbonated; (**b**) 1 h carbonated sample; (**c**) 9 h carbonated sample.
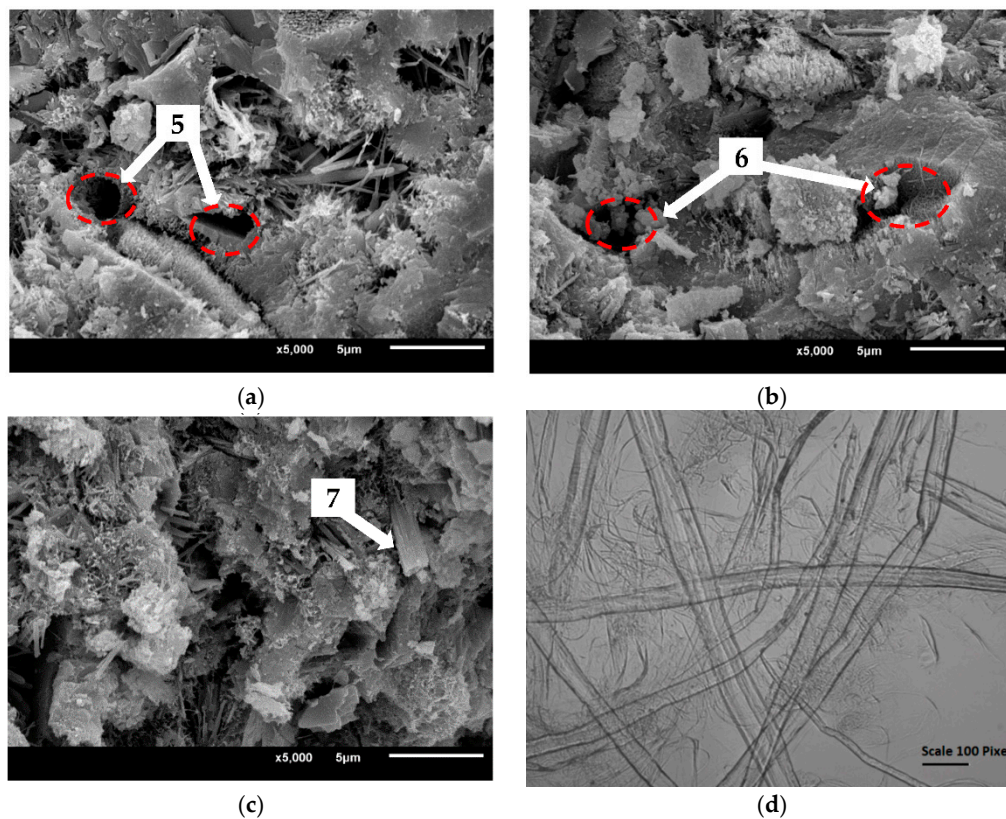
Figure 13. Scanning electron micrographs on a fractured sample of fiber-cement composites (**a**) non-carbonated; (**b**) 1 h carbonated sample; (**c**) 9 h carbonated sample; (**d**) refined fibers containing a large number of filaments.

SEM analysis of fractured samples allows observations of the changes of fiber-matrix bond (i.e., ITZ) and how deep the samples were carbonated. The fractures were prepared at the age of 28 days within 1 mm distance from the surface. Figure 13a shows the micrograph of a fractured non-carbonated sample, which exhibited poor bonding between the fiber and matrix. As a result, the fiber was pulled out during fracture preparation, which created holes (dashed ellipse) on the fracture as shown by Arrow 5 in Figure 13a. After 1 h carbonation curing, calcite precipitated around the interfacial transition zone between the fiber and matrix and other pores. Therefore, there appeared some calcites precipitated around the holes (dashed ellipse) created due to the pulling out of fibers, as indicated by Arrow 6 in Figure 13b. Figure 13c shows a better fiber-matrix bonding, which prevented the fibers pulling out from the matrix. Arrow 7 was a filament of cellulose fiber, which was kept in the matrix during SEM fractured sample preparation. This indicates that carbonation helped create a better adhesion of fiber and cement matrix because of the refinement of composite microstructure. Note that the fibers used in this study were refined ones, which contain a large number of filaments as shown in Figure 13d. These filaments had sizes (diameter) ranging from 1 micron to 30 microns, which are shown in Figure 13c.

4. Discussion on Optimal Carbonation Curing Conditions and Enhanced ITZ

The carbonation curing period plays an important role in the changes of physical and mechanical properties of composites. A curing period of less than 3 h resulted in significant effects on the bulk density, modulus of rupture, modulus of elasticity, and toughness. Under semi-adiabatic conditions, the temperature in the curing chamber gradually increased to 60 °C during this period (see Figure 5). If we stop the carbonation directly after 3 h curing, heat and moisture loss could occur resulting in less hydration and degree of carbonation. However, at longer curing times, the results show that the

carbonation improved the mechanical and physical properties, except for toughness because of its inverse relationship with MOE as described earlier (see also Figure 11a). In addition, the water content has a significant impact on the carbonation curing process. The higher the rolling pressure, the better the physical and mechanical properties. However, increasing rolling pressure higher than 5 bar induced a significant drop in toughness, which results in the composites not meeting the minimum requirement for toughness. Higher rolling pressure up to a certain value slowed down the carbonation rate because of the retention process resulting from the decrease of apparent void volume and density, which lowered the diffusion and permeability of CO_2. As a result, the carbonation efficiency decreased as shown in Figures 8 and 9.

Increasing CO_2 pressure indeed has a positive impact on the carbonation process because it increases the concentration of CO_2 in both gas and aqueous phases to carbonate the cementitious matrix. We see in Figure 6a that the MOR does not improve when the carbonation curing time lasts longer in the case of 1 bar CO_2 pressure. However, the MOR significantly increased when the CO_2 pressure increased to 3 bar.

The SEM microstructural analysis helps to understand how the accelerated carbonation process improves the contact between filaments of cellulose fiber and cement matrix by favoring a better adhesion between them. However, note that higher fiber-matrix bond could have negative effects on the toughness and flexibility of fiber-cement composites. The matrix around the fiber has a porosity gradient with lower and higher density regions than the bulk paste matrix as illustrated in Figure 14. This is because of the fact that (cellulose) fiber can absorb water and thus increase the water to cement ratio surrounding the fiber, which results in a higher porosity region during cement hydration. Therefore, the fibers are easily pulled out under mechanical forces during the fractured sample preparation for SEM analysis as shown in Figure 13a. These weak regions have been improved thanks to carbonation. The development of the microstructure as the carbonation advanced results in a reaction zone containing a considerable volume of calcium carbonate crystals, which tend to deposit in large cavities or regions with higher porosity. Analysis of SEM images (Figure 13c) could prove the presence of a reaction zone characterized by the precipitation of calcite in the pores in the interfacial transition zone (ITZ) between the fibers and cement matrix (Figure 14).
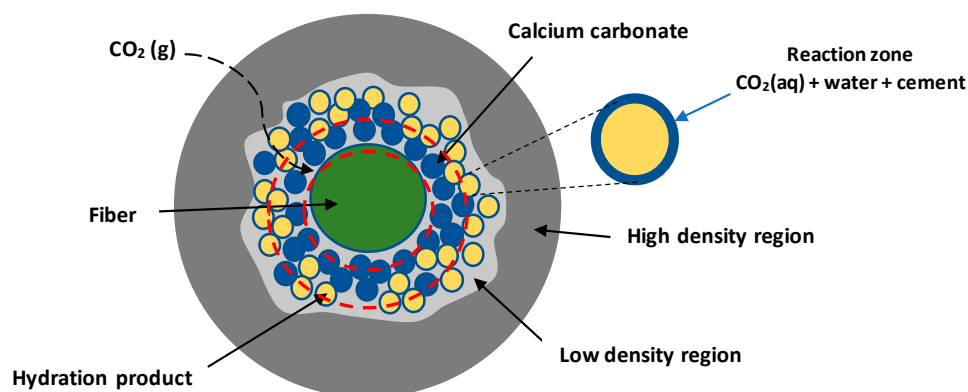
Figure 14. Schematic illustration of the fiber and matrix adapted from [16]—interfacial transition zone (ITZ) is represented by the zone between the two red dashed circles.

5. Conclusions and Perspectives

In this study, we performed a parametric investigation of the effects of carbonation curing conditions, which included CO_2 pressure, rolling pressure, and curing period on the changes to the physical and mechanical properties because of carbonation under close to real manufacturing conditions. Though correlations exist (linear or non-linear) between different influencing factors, we can conclude that the fiber-cement composites cured with high CO_2 concentration of 3 bar, rolling

pressure of 3 bar, and 5 h of curing time provided optimal curing conditions resulting in the most desirable properties, which are (i) modulus of rupture; (ii) modulus of elasticity; (iii) air void volume; (iv) bulk density; and (v) water absorption. However, the toughness was greatly reduced when increasing the CO_2 pressure, curing time, and rolling pressure. In addition, there was evidence from SEM analysis that carbonation curing improved the fiber-cement matrix bond by the precipitation of carbonation products in the pores in the interfacial transition zone between the fibers and the cement matrix. Longer carbonation times improved the fiber-matrix interface.

In order to investigate in more detail, the interactions between different influencing parameters, a factorial experimental program could be carried out in the future. Along with this, a modelling approach would help optimize the curing conditions and enable better understanding of the changes in mechanical and physical properties. In this sense, once curing conditions are optimized, the carbonation curing of fiber-cement composites under elevated CO_2 conditions could enhance the mechanical properties as well as resulting in environmentally beneficial effects by reducing carbon dioxide emission by recycling CO_2 released from industrial activities (such as cement manufacture).

Author Contributions: Bundit Kottititum designed and performed the experiments, and drafted the paper. Quoc Tri Phung analyzed the data and revised the paper. Wichit Prakaypan performed SEM experiments and proposed mix compositions of the fiber-cement composites. Thongchai Srinophakun and Norbert Maes made suggestions that contributed to improve the manuscript.

Conflicts of Interest: The authors declare no conflict of interest.

References

1. Ikai, S.; Reichert, J.R.; Rodrigues, A.V.; Zampieri, V.A. Asbestos-free technology with new high toughness polypropylene (PP) fibers in air-cured Hatschek process. *Constr. Build. Mater.* **2010**, *24*, 171–180. [CrossRef]

2. Brandt, A.M. *Cement-Based Composites: Materials, Mechanical Properties and Performance*; CRC Press: Boca Raton, FL, USA, 2009.

3. Zhou, X.; Li, Z. Characterization of rheology of fresh fiber reinforced cementitious composites through ram extrusion. *Mater. Struct.* **2005**, *38*, 17–24. [CrossRef]

4. Li, Z.; Mobasher, B.; Shah, S.P. Characterization of Interfacial Properties in Fiber-Reinforced Cementitious Composites. *J. Am. Ceram. Soc.* **1991**, *74*, 2156–2164. [CrossRef]

5. Mechtcherine, V.; Slowik, V.; Kabele, P. *Strain-Hardening Cement-Based Composites: SHCC4*; Springer: Berlin, Germany, 2017; Volume 15.

6. Balaguru, P.N.; Shah, S.P. *Fiber-Reinforced Cement Composites*; McGraw-Hill: New York, NY, USA, 1992.

7. Benson, S.M.; Orr, F.M. Carbon dioxide capture and storage. *Mrs Bull.* **2008**, *33*, 303–305. [CrossRef]

8. Leung, D.Y.; Caramanna, G.; Maroto-Valer, M.M. An overview of current status of carbon dioxide capture and storage technologies. *Renew. Sustain. Energy Rev.* **2014**, *39*, 426–443. [CrossRef]

9. Phung, Q.T.; Maes, N.; Jacques, D.; Bruneel, E.; Van Driessche, I.; Ye, G.; De Schutter, G. Effect of limestone fillers on microstructure and permeability due to carbonation of cement pastes under controlled CO_2 pressure conditions. *Constr. Build. Mater.* **2015**, *82*, 376–390. [CrossRef]

10. Phung, Q.T.; Maes, N.; Jacques, D.; De Schutter, G.; Ye, G. Effect of Limestone Fillers on Ca-Leaching and Carbonation of Cement Pastes. *Key Eng. Mater.* **2016**, *711*, 269–276. [CrossRef]

11. Pacheco-Torgal, F.; Jalali, S. Cementitious building materials reinforced with vegetable fibres: A review. *Constr. Build. Mater.* **2011**, *25*, 575–581. [CrossRef]

12. Urrea-Ceferino, G.E.; Rempe, N.; dos Santos, V.; Junior, H.S. Definition of optimal parameters for supercritical carbonation treatment of vegetable fiber-cement composites at a very early age. *Constr. Build. Mater.* **2017**, *152*, 424–433. [CrossRef]

13. Phung, Q.T. Effects of Carbonation and Calcium Leaching on Microstructure and Transport Properties of Cement Pastes. Ph.D. Thesis, Department of Structural Engineering, Ghent University, Ghent, Belgium, 2015; p. 249.

14. Bertos, M.F.; Simons, S.J.R.; Hills, C.D.; Carey, P.J. A review of accelerated carbonation technology in the treatment of cement-based materials and sequestration of CO_2. *J. Hazard. Mater.* **2004**, *112*, 193–205.

15. Rostami, V.; Shao, Y.; Boyd, A.J. Durability of concrete pipes subjected to combined steam and carbonation curing. *Constr. Build. Mater.* **2011**, *25*, 3345–3355. [CrossRef]

16. Santos, S.F.; Schmidt, R.; Almeida, A.E.; Tonoli, G.H.; Savastano, H. Supercritical carbonation treatment on extruded fibre–cement reinforced with vegetable fibres. *Cem. Concr. Compos.* **2015**, *56*, 84–94. [CrossRef]

17. Ghoshal, S.; Kashef-Haghighi, S. CO_2 Sequestration in Concrete through Accelerated Carbonation Curing in a Flow-through Reactor. *Ind. Eng. Chem. Res.* **2010**, *49*, 1143–1149.

18. Yu, C.-H.; Huang, C.-H.; Tan, C.-S. A review of CO_2 capture by absorption and adsorption. *Aerosol Air Qual. Res.* **2012**, *12*, 745–769. [CrossRef]

19. Walton, J.C.; Bin-Shafique, S.; Smith, R.W.; Gutierrez, N.; Tarquin, A. Role of carbonation in transient leaching of cementitious wasteforms. *Environ. Sci. Technol.* **1997**, *31*, 2345–2349. [CrossRef]

20. Fattuhi, N. Concrete carbonation as influenced by curing regime. *Ceme. Concr. Res.* **1988**, *18*, 426–430. [CrossRef]

21. Liu, L.; Ha, J.; Hashida, T.; Teramura, S. Development of a CO_2 solidification method for recycling autoclaved lightweight concrete waste. *J. Mater. Sci. Lett.* **2001**, *20*, 1791–1794. [CrossRef]

22. Almeida, A.E.F.S.; Tonoli, G.H.D.; Santos, S.F.; Savastano, H. Improved durability of vegetable fiber reinforced cement composite subject to accelerated carbonation at early age. *Cem. Concr. Compos.* **2013**, *42*, 49–58. [CrossRef]

23. Pizzol, V.; Mendes, L.M.; Frezzatti, L.; Savastano, H., Jr.; Tonoli, G.H.D. Effect of accelerated carbonation on the microstructure and physical properties of hybrid fiber-cement composites. *Miner. Eng.* **2014**, *59*, 101–106. [CrossRef]

24. Scrivener, K.L.; Crumbie, A.K.; Laugesen, P. The interfacial transition zone (ITZ) between cement paste and aggregate in concrete. *Interface Sci.* **2004**, *12*, 411–421. [CrossRef]

25. Da Costa Correia, V.; Santos, S.F.; Teixeira, R.S.; Junior, H.S. Nanofibrillated cellulose and cellulosic pulp for reinforcement of the extruded cement based materials. *Constr. Build. Mater.* **2018**, *160* (Suppl. C), 376–384. [CrossRef]

26. Lee, S.-K.; Jeon, M.J.; Cha, S.S.; Park, C.G. Mechanical and Permeability Characteristics of Latex-Modified Fiber-Reinforced Roller-Compacted Rapid-Hardening-Cement Concrete for Pavement Repair. *Appl. Sci.* **2017**, *7*, 694. [CrossRef]

27. Ranjbar, N.; Talebian, S.; Mehrali, M.; Kuenzel, C.; Metselaar, H.S.C.; Jumaat, M.Z. Mechanisms of interfacial bond in steel and polypropylene fiber reinforced geopolymer composites. *Compos. Sci. Technol.* **2016**, *122*, 73–81. [CrossRef]

28. Morton, J.H.; Cooke, T.; Akers, S. Performance of slash pine fibers in fiber cement products. *Constr. Build. Mater.* **2010**, *24*, 165–170. [CrossRef]

29. Yoon, S.-H.; Van Heiningen, A. Kraft pulping and papermaking properties of hot-water pre-extracted loblolly pine in an integrated forest products biorefinery. *TAPPI J.* **2008**, *7*, 22–27.

30. Portland Cement Association. ASTM C 150, Type I or II, except Type III may be used for cold-weather construction. In *Provide Natural Color or White Cement as Required to Produce Mortar Color Indicated*; PCA: Skokie, IL, USA, 1993; Volume 1.

31. Bentur, A.; Akers, S. The microstructure and ageing of cellulose fibre reinforced cement composites cured in a normal environment. *Int. J. Cem. Compos. Lightweight Concr.* **1989**, *11*, 99–109. [CrossRef]

32. Cooke, T. Formation of films on Hatschek machines. In Proceedings of the 8th Conference on Inorganic-Bonded Wood and Fiber Composite Materials, Sun Valley, ID, USA, 23–25 September 2002.

33. ASTM C948-81. *Standard Test Method for Dry and Wet Bulk Density, Water Absorption, and Apparent Porosity of thin Sections of Glass-Fibre Reinforced Concrete1*; American Society for Testing and Materials: West Conshohocken, PA, USA, 2001.

34. Peter, M.; Muntean, A.; Meier, S.A.; Böhm, M. Competition of several carbonation reactions in concrete: A parametric study. *Cem. Concr. Res.* **2008**, *38*, 1385–1393. [CrossRef]

35. Borges, P.H.; Costa, J.O.; Milestone, N.B.; Lynsdale, C.J.; Streatfield, R.E. Carbonation of CH and C–S–H in composite cement pastes containing high amounts of BFS. *Cem. Concr. Res.* **2010**, *40*, 284–292. [CrossRef]

36. Phung, Q.T.; Maes, N.; Jacques, D.; De Schutter, G.; Ye, G. Investigation of the changes in microstructure and transport properties of leached cement pastes accounting for mix composition. *Cem. Concr. Res.* **2015**, *79*, 217–234. [CrossRef]

37. Soroushian, P.; Aouadi, F.; Chowdhury, H.; Nossoni, A.; Sarwar, G. Cement-bonded straw board subjected to accelerated processing. *Cem. Concr. Compos.* **2004**, *26*, 797–802. [CrossRef]

38. Tonoli, G.; Rodrigues Filho, U.P.; Savastano, H.; Bras, J.; Belgacem, M.N.; Lahr, F.R. Cellulose modified fibres in cement based composites. *Compos. Part A Appl. Sci. Manuf.* **2009**, *40*, 2046–2053. [CrossRef]

39. Phung, Q.T.; Maes, N.; De Schutter, G.; Jacques, D.; Ye, G. A methodology to study carbonation of cement paste and its effect on permeability. In Proceedings of the 4th International Conference on Accelerated Carbonation for Environmental and Materials Engineering (ACEME-2013), Leuven, Belgium, 9–12 April 2013.

40. Phung, Q.T.; Maes, N.; Jacques, D.; De Schutter, G.; Ye, G.; Perko, J. Modelling the carbonation of cement pastes under a CO_2 pressure gradient considering both diffusive and convective transport. *Constr. Build. Mater.* **2016**, *114*, 333–351. [CrossRef]

41. E Silva, A.C.; Junior, H.S.; John, V.M. Aging of composites based on blast furnace slag and reinforced with eucalyptus residual cellulose pulp. *Ambiente Construído* **2009**, *9*, 25–44.

42. Kashef-Haghighi, S.; Shao, Y.; Ghoshal, S. Mathematical modeling of CO_2 uptake by concrete during accelerated carbonation curing. *Cem. Concr. Res.* **2015**, *67*, 1–10. [CrossRef]

43. Phung, Q.T.; Maes, N.; Jacques, D.; De Schutter, G.; Ye, G. Evolution of Microstructure and Transport Properties of Cement Pastes Due to Carbonation under a CO_2 Pressure Gradient—A Modeling Approach. In *CONCREEP 10*; Hellmich, C., Pichler, B., Kollegger, J., Eds.; American Society of Civil Engineers: Ritton, VA, USA, 2015; pp. 1032–1041.

44. Mahaphant Fibre-Cement Public Company Limited. *Technical Data of Mahaphant Fibre Cement Roof Covering Products*; Mahaphant Fibre-Cement Public Company Limited: Lopburi, Thailand, 2014; p. 12.

45. Chen, X.; Wu, S.; Zhou, J. Influence of porosity on compressive and tensile strength of cement mortar. *Constr. Build. Mater.* **2013**, *40*, 869–874. [CrossRef]

46. Adamopoulos, S.; Passialis, C. Relationship of toughness and modulus of elasticity in static bending of small clear spruce wood specimens. *Eur. J. Wood Wood Prod.* **2010**, *68*, 109–111. [CrossRef]